Biophysical Journal Volume 101 October 2011 1887–1895

The Structural Pathway for Water Permeation through Sodium-Glucose Cotransporters

Louis J. Sasseville,[†△] Javier E. Cuervo,[‡△] Jean-Yves Lapointe,[†*] and Sergei Y. Noskov[‡]
[†]Groupe d'étude des protéines membranaires and Département de Physique, Université de Montréal, Montréal, Québec, Canada; and [‡]Institute for Biocomplexity and Informatics and Department of Biological Sciences, University of Calgary, Calgary, Alberta, Canada

ABSTRACT Although water permeation across cell membranes occurs through several types of membrane proteins, the only permeation mechanism resolved at atomic scale is that through aquaporins. Crystallization of the *Vibrio parahaemolyticus* sodium-galactose transporter (vSGLT) allows investigation of putative water permeation pathways through both vSGLT and the homologous human Na-glucose cotransporter (hSGLT1) using computational methods. Grand canonical Monte Carlo and molecular dynamics simulations were used to stably insert water molecules in both proteins, showing the presence of a water-filled pathway composed of ~100 water molecules. This provides a structural basis for passive water permeation that is difficult to reconcile with the water cotransport hypothesis. Potential-of-mean-force calculations of water going through the crystal structure of vSGLT shows a single barrier of 7.7 kCal mol^{-1}, in agreement with previously published experimental data for cotransporters of the SGLT family. Electrophysiological and volumetric experiments performed on hSGLT1-expressing *Xenopus* oocytes showed that the passive permeation pathway exists in different conformational states. In particular, experimental conditions that aim to mimic the conformation of the crystal structure displayed passive water permeability. These results provide groundwork for understanding the structural basis of cotransporter water permeability.

INTRODUCTION

Water transport across biological membranes is one of the most basic physiological processes occurring in living cells. In addition to simple diffusion through the lipid bilayer and facilitated transport through aquaporins, a number of membrane proteins that transport other substrates were also shown to mediate water permeation. One of the first measurements of transporter-related water permeation across glucose-facilitated transporters was published in 1989 (1). Later, the Na/glucose cotransporter (SGLT1), which is responsible for Na/glucose cotransport in the intestine and in renal late proximal tubules, was also found to be water-permeable (2,3). SGLT1 was the first cloned member of the SLC5 gene family—a family that includes the Na-coupled transporters for sugars, myo-inositol, monocarboxylates, iodide, vitamins, and choline (4). Several laboratories have reported that expressing SGLT1 in *Xenopus laevis* oocytes produced a twofold increase in passive water permeability, which returned to the level found in noninjected oocytes upon addition of phlorizin (Pz), a specific SGLT1 inhibitor (2,5,6). Although the passive water permeability of SGLT1 is well accepted, the ability of SGLT1 to mediate secondary active water transport has been debated for a decade (7,8).

Based on the observation that addition of glucose to an oocyte-expressing SGLT1 is accompanied, within 5–20 s, by a readily detectable cell swelling, some researchers have proposed the *water cotransport hypothesis*, which stipulates that SGLT1 physically couples the transport of two Na^+ ions with one glucose molecule and some 250–400 water molecules (9,10). Alternatively, we have argued that all water transport must, in fact, be passive because a transport-dependent osmotic gradient of the appropriate amplitude could be detected across the oocyte membrane as soon as 20 s after adding glucose (5,11,12). The recent crystallization of the SGLT bacterial homolog *Vibrio parahaemolyticus* sodium-galactose transporter (vSGLT) by Faham et al. (13) allows investigation of the water pathway across the cotransporter at a molecular level by using atomistic simulations—helping us to resolve longstanding questions regarding the mechanism of transporter-mediated water permeation. In the case of vSGLT, it is worth noting that no experimental data exist about its water permeability; this is probably due to poor expression level in *Xenopus* oocytes (14).

In this article, we used homology modeling, grand canonical Monte Carlo (GCMC) simulations, molecular dynamics, and potential-of-mean-force calculations to unveil the molecular mechanism of water permeation through the transporter. The relevance of the identified passive permeation pathway was then experimentally confirmed for the different conformational states of human SGLT1 (hSGLT1) that can be reached by changing membrane potential and external Na concentrations.

METHODS

Molecular dynamics, grand canonical Monte Carlo and potential-of-mean-force calculations

We have performed molecular dynamics (MD), grand canonical Monte Carlo (GCMC) simulations, and potential-of-mean force (PMF) calculations to explore the existence of water permeation pathways in

Submitted April 1, 2011, and accepted for publication September 16, 2011.
△Louis J. Sasseville and Javier E. Cuervo contributed equally to this work.
*Correspondence: jean-yves.lapointe@umontreal.ca
Editor: Hassane Mchaourab.

0006-3495/11/10/1887/9 $2.00
doi: 10.1016/j.bpj.2011.09.019

two models, namely the available open-inward vSGLT crystal structure and a homology model that we built for human SGLT1 (hSGLT1), which shares 32% identity (60% similarity) with the amino-acid sequence of vSGLT (13).

The starting configuration for vSGLT was taken from the x-ray coordinates published by Faham et al. (13) (PDB ID: 3DH4, Chain A) and was reoriented based on the orientation-of-membrane-proteins database, OPM (15). An hSGLT1 homology model based on the published sequence alignment (13) was generated using the SCWRL web-server (16). The sequence identity is sufficient for credible homology modeling (17,18). Furthermore, the identity found in the TM segments that play important roles in the water pathway is even higher, thereby ensuring the relevance of the constructed model. The sequence identity between hSGLT1 and vSGLT is 34% and 40% for TM2 and TM6, respectively (see also Fig. 3 *C*).

Both protein systems were embedded in a lipid membrane using a multistep membrane-building procedure (CHARMM-GUI) described before (19–21). The simulation box contained the transporter, bound sodium ions, one substrate, and ~110 lipid molecules (1-palmitoyl-2-oleoyl-*sn*-glycero-3-phosphocholine) solvated in an explicit 100 mM NaCl aqueous solution. A snapshot of the full simulation box is shown in Fig. 1 *A*. All GCMC/MD computations were carried out using CHARMM version c35b1 with the CHARMM27 force fields for proteins and lipids (22). MD simulation methods were similar to those used in previous studies of membrane systems (19). Briefly, constant temperature/constant pressure algorithms were applied (with pressure at 1 atm and temperature at 315 K). Periodic boundary conditions were used for the rectangular system. Electrostatic interactions were treated with the particle-mesh Ewald algorithm with a 96 Å × 96 Å × 96 Å grid for fast Fourier transform, $\kappa = 0.34$ Å^{-1} and a sixth-order spline interpolation. The nonbonded interactions were smoothly switched off at 12–14 Å. Each simulation system was equilibrated for 3 ns without any configurational constraints. Additionally, to test the stability of the homology model, we performed an equilibrium MD simulation of 15 ns at 345 K. During the length of this simulation the model remained stable, secondary structure domains were preserved, and the RMSD of the alpha-carbon atoms plateaued at ~4 Å.

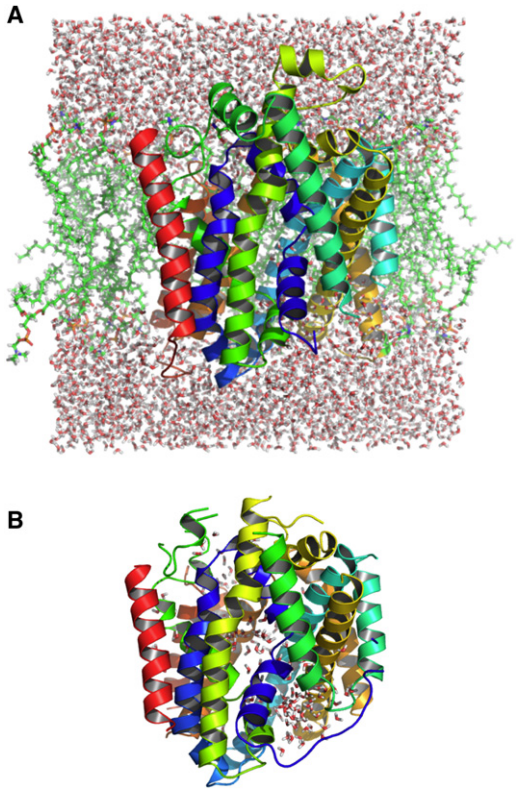

FIGURE 1 (*A*) Complete equilibrium MD system and (*B*) reduced GCMC/MD system, both for the crystal structure of vSGLT.

After the equilibrium MD simulations, GCMC simulations were performed to stably insert water molecules inside the models (23). The general principles of a GCMC simulation can be explained as follows: GCMC allows variation of the number of particles in the system, in this case water, while keeping the chemical potential constant. In our methodology, this is done in an area of interest that is explicitly treated while the rest of the system is mapped into a continuous model. In this case, we focused on the region of the system that is centered on the sugar binding site. Within the GCMC framework, water molecules are randomly inserted or deleted following a Metropolis algorithm. Therefore, based on the change in net free energy after insertion or deletion of a water molecule, the new conformation will be either accepted or rejected.

Only the atoms located within 20 Å of the sugar binding site were treated explicitly. All other atoms in the system were considered implicitly using a generalized solvent boundary potential (GSBP) (24) generated for each system. It has been shown that the use of GSBP significantly decreases the size of the system (in our case from ~40,000 to ~7000 atoms, Fig. 1 *B*) while keeping treatment of dynamics in the explicitly treated part of the system, reasonably accurate (25). After the GSBP maps were generated, the reduced systems were minimized and equilibrated for 0.5 ns. For GCMC simulations, models of hSGLT1 and vSGLT transporters were set to be ligand-free, i.e., neither sugar nor ions were present for the GCMC cycles. We have used recommended values for acceptance probabilities, translational and rotational moves, and excess chemical potential of water molecules (~6 kcal/mol in accordance with data on TIP3P water) (23). A short Langevin dynamics run of 10 ps was used to relax the protein structure around an inserted water molecule, thus accounting for local flexibility and removing steric clashes. Each MC cycle consisted of 100 minimization steps and it was determined by trial and error that at least 100 MC cycles needed to be performed for full saturation to be achieved.

To complement our GCMC study, we calculated the potential of mean force along the water permeation path of vSGLT. To this end, we calculated the spatial water density ($G(x, y, z)$) in the simulation box. A 225-ns MD simulation of the whole system was carried out to sample the position of water. The trajectory was postprocessed and the three-dimensional water density was calculated. We used a cubic grid with voxels of 125 Å^3. This volume corresponds to roughly four-times the volume occupied by a single water molecule. The cell unit volume was chosen so that it would be possible to fit two water molecules along the diagonal of a voxel. To calculate the PMF, an algorithm was implemented to find and follow all possible paths that go from the extracellular side to the intracellular side of the membrane. We define a path as a collection of continuous voxels with a density value > 0 that also hold the following conditions: 1), the position of each voxel in the path changes by one unit in the Z direction toward the intracellular side, and 2), the difference between the X and Y positions of two contiguous voxels cannot be larger than one unit cell. Once all possible continuous paths were identified, the PMF was calculated based on the average density ($G(x, y, z)_{ave}$) over all continuous paths as

$$PMF(z) = -KT \ln\left(\frac{G(x,y,z)_{ave}}{G(x,y,z)_{bulk}}\right),$$

where $G(x, y, z)_{bulk}$ is the average density of the bulk water region along the path. Because the position in the Z direction of the path increases monotonically by one unit cell, the calculated PMF is effectively the projection of the three-dimensional PMF along the z axis.

Oocyte preparation and injection

Oocytes were surgically removed from *X. laevis* frogs and were defolliculated as described previously (26). One or two days after defolliculation, healthy oocytes were injected with 46 nL of water containing mRNA

coding for myc-tagged human SGLT1 (0.1 μg/μL). As shown previously (26), this N-terminus epitope-tagged version of SGLT1 displays properties that are indistinguishable from the untagged form.

Solutions

Isotonic solutions for volumetric and electrophysiological experiments contained: 67.5 mM NaCl, 3 mM KCl, 0.82 mM $MgCl_2$, 0.74 mM $CaCl_2$, 5 mM HEPES (pH adjusted to 7.6 with 2 M Tris), and 50 mM mannitol (final osmolality of 197 mOsm/kg H_2O). Hypotonic solutions were obtained by removing 50 mM mannitol (final osmolality of 147 mOsm/kg H_2O. A quantity of 200 μM Pz (Sigma, St. Louis, MD) was directly added to hypotonic solutions from a concentrated stock solution in ethanol (500 mM). Na-free hypotonic solution was obtained by replacing 67.5 mM NaCl with 67.5 mM *n*-methyl-D-glucamine-Cl (NMDG-Cl) (Sigma). The osmolality of each solution was controlled within 1 mOsm/kg H_2O using a vapor pressure osmometer (Advanced DigiMatic Osmometer, model 3D2; Advanced Instruments, Norwood, MA). For all experimental protocols, oocytes were equilibrated for at least 20 min in isotonic solution to obtain a stable volume measurement.

Optical and electrophysiological measurement

Water permeability was evaluated by optical measurements on oocytes challenged with hypotonic media. Details of the procedure are given in previous publications dealing with SGLT1 and water transport (5,10,27). Briefly, the experimental chamber (volume of 0.07 ml) was specifically designed to enable rapid solution changes (solution flux of 1.2 ml/min), thus allowing measurement of rapid changes in oocyte volume. The oocyte was illuminated from above with a light-emitting diode dipped in the bath solution and high-contrast images were captured with a charge-coupled device camera attached to an inverted microscope equipped with a 3× objective. Oocyte volume was calculated from its cross section measured 30 times/s with custom-made pixel counting software. Two-microelectrode voltage-clamp experiments and data acquisition were carried out as described previously (28). Oocytes were equilibrated for at least 20 min in isotonic solution before impalement. Once impaled, the appropriate holding potential was imposed and an isotonic solution was superfused. Both measured current and volume were allowed to stabilize before the actual trial was initiated (typically ~5 min). A typical assay is shown later in Fig. 5 *A*.

Because *trans*-membrane water movement decreases the local osmotic gradient, water fluxes decrease with time. In addition to using short time durations for the different experimental conditions (60 s for each), we circumvented this problem by bracketing a given experimental condition by two identical control conditions. For example, in Fig. 5 *A* where the effect of membrane potential on water permeability was tested, the oocyte was held at −100 mV, then at −20 mV, and then at −100 mV (corresponding to experimental conditions *pre*, *exp*, and *post*, respectively). The value for the swelling rate at −100 mV was taken as the mean of the *pre* and *post* conditions and was compared to the swelling rate measured at −20 mV. In trials assessing the effect of Na, the term *exp* corresponded to a Na-free solution, whereas *pre* and *post* were in the presence of 67.5 mM Na. At the end of each trial, Pz was added to the bath to assess the oocyte's expression level. Because water permeability of an individual oocyte depends upon the level of expression of hSGLT1, paired measurements were performed. To control for possible effects of external Na or V_m on the endogenous water permeability, the two protocols were also applied to noninjected oocytes.

The water permeability (P_f) of the oocyte was calculated using the swelling rate resulting from a hypotonic shock according to the relation (27,29)

$$P_f = \frac{1}{S \times v_W \times \Delta\pi} \frac{dV}{dt}, \quad (1)$$

where S is a standard oocyte surface of 0.4 cm^2 (assuming a membrane infolding factor of 9) (30), v_W is the specific volume of water (18.2 cm^3/mol), $\Delta\pi$ represents the size of the hypotonic shock (50 mOsm in the case of this study), and dV/dt is the swelling rate (i.e., the slope of the volume versus time curve).

RESULTS

Although sequence homology between vSGLT and hSGLT1 is reasonably high, the spatial localization of water insertion regions obtained for the two proteins are slightly different. The GCMC simulations produced a discontinuous water permeation pathway in vSGLT, displaying a 14 Å gap in the external half of the protein, centered at ~10 Å above the ligand binding site (see Fig. 2 *A*), while a stable, quasi-continuous water pathway was readily identified in the hSGLT1 model (see Fig. 2 *B*).

The hSGLT1 homology model displays a water permeation pathway extending from the intra- to the extracellular side. This pathway goes through the intracellular vestibule and the sugar binding site, but does not follow the putative substrate pathway in the region between the sugar binding site and the external face of the cotransporter. If TM

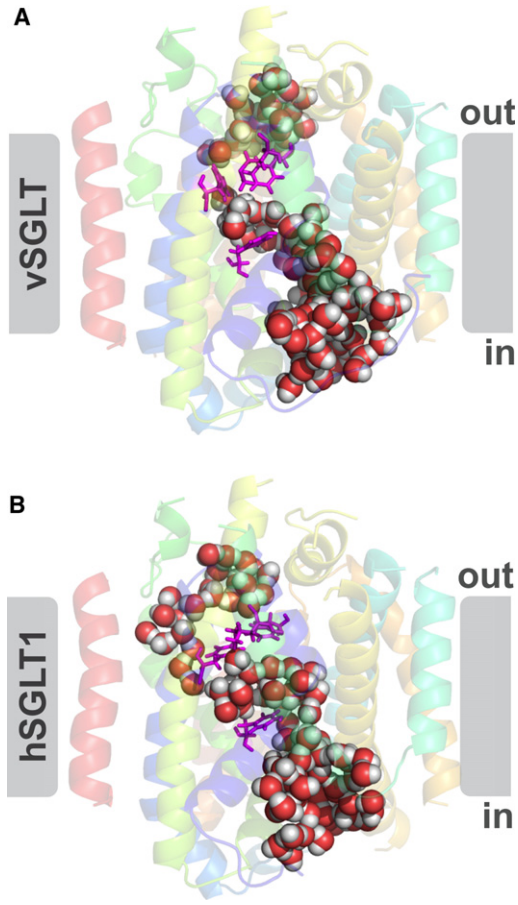

FIGURE 2 Water permeation pathway through vSGLT (*A*) and hSGLT1 (*B*). Hydrophobic plug residues (*stick representation*). Only relevant water molecules are shown.

segments are numbered according to the LeuT nomenclature (where vSGLT's N-terminal TM segment becomes TM−1, the next becomes TM1, and so forth), the putative substrate pathway is proposed to go through the extracellular hydrophobic plug formed by TM 1, 2, and 10 (13), whereas the proposed water permeation pathway found in the this study runs parallel to this and goes through the four-helix bundle formed by TM1, 2, 6, and 7 (see Fig. S1 in the Supporting Material).

In this region of hSGLT1, a structural constriction reduces the permeation pathway to a single-file water chain followed by a 4.3 Å gap of low water density (Fig. 3 *B*). This gap may indicate the presence of a structural barrier to the formation of a continuous water permeation pathway across hSGLT1. The barrier is formed by a specific group of residues, namely: Phe-101, Ala-105 (TM2), Met-283, Leu-286, Thr-287 (TM6E), and Gln-455 (TM10). Examination of water-insertion zones suggests that this water-depleted region is not due to possible steric clashes, because sufficient space to accommodate additional water molecules was found to be available.

Similar to the results of MD and GCMC/MD simulations done on hSGLT1, the equilibrated vSGLT structure exhibits hydration of the intracellular and extracellular vestibules. However, only part of the extracellular-side pathway found in the hSGLT1 system is conserved (Fig. 2 *A*). The structure of vSGLT cannot accommodate stable water molecules in the general area corresponding to the constriction zone found in hSGLT1. Comparison with the constriction found in hSGLT1 allowed identification of the relevant residues of vSGLT in or around this discontinuity: Tyr-87 (TM2), Ala-259 (TM6E), Gln-425, Gln-428 (TM10), Phe-479, and Met-483 (TM12) (see Fig. 3 *A*).

To further characterize the proposed water permeation pathway, we calculated the PMF of water going from one side of the membrane to the other. We followed the methodology described in Methods, above. The implemented methodology is based on extensive (225 ns) MD sampling of the position of water, to estimate the spatial water density. It is generally accepted that results from rather long MD simulations of homology models are not sufficiently reliable to draw strong conclusions about the structure or function of proteins. Therefore, we limited the calculation of PMF to the available crystal structure of vSGLT. The obtained PMF is shown in Fig. 4. A single barrier of 7.7 kcal mol^{-1} is observed at approximately the center of the membrane. The position coincides with the dry zone observed in the

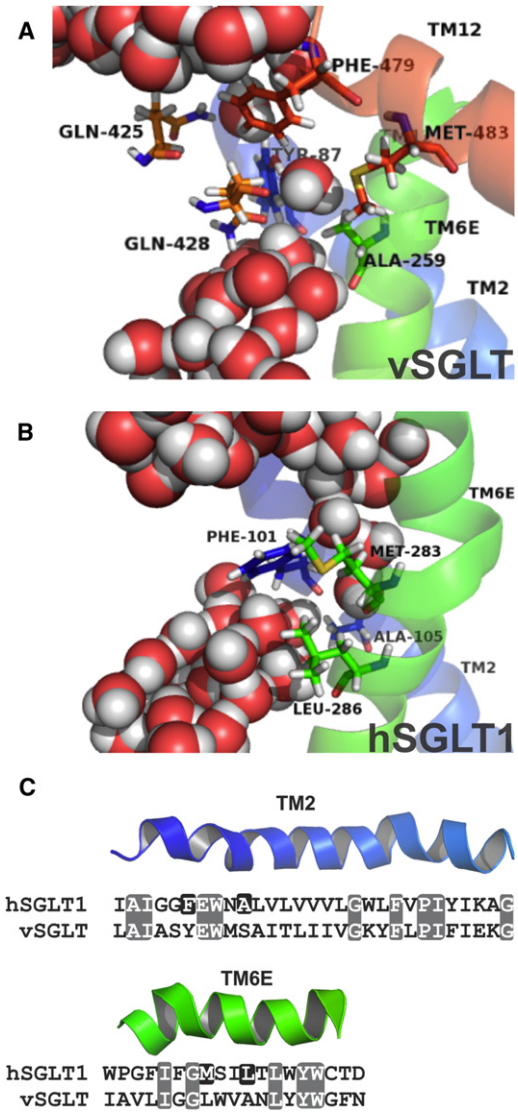

FIGURE 3 Comparison of the constriction areas in hSGLT1 and vSGLT. (*A*) Relevant residues surrounding discontinuity in vSGLT. (*B*) Hydrophobic residues surrounding the 4.3 Å gap in the hSGLT1-mediated water pathway. (*C*) Sequence alignment of TM2 and TM6E. (*Shading*) Conserved residues; (*solid*) relevant residues for this work. Adapted from Faham et al. (13). Transmembrane segments are numbered according to LeuT nomenclature.

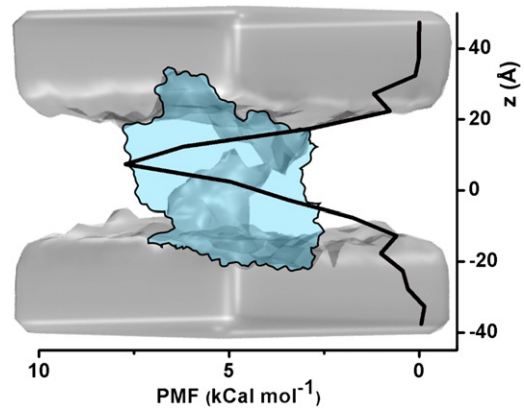

FIGURE 4 Potential of mean force (PMF) profile for vSGLT. Values were projected onto the *z* axis, which is defined as being perpendicular to the membrane. Origin of *z* axis corresponds roughly to the substrate binding zone. The PMF profile is superimposed onto a surface representation of the water density and a silhouette representation of vSGLT, using the same general orientation as shown in Fig. 3 *A*.

GCMC calculation. However, more exhaustive sampling shows that the water permeation path can be indeed continuous. The value of the calculated energy barrier is in very good agreement with the activation energies of 9 ± 1 and 5 ± 1 kcal mol^{-1}, which have been measured in the presence of Na and absence of sugar for rabbit SGLT1 (3,6).

The proposed structure for the water pathway of Na/glucose cotransporters was obtained in the single conformational state presently available for vSGLT (inward-facing galactose-bound configuration). To assess the relevance of the identified water pathway during the different conformational states reached during cotransport, we measured hSGLT1 water permeability in the presence or absence of extracellular Na and at different membrane potentials. In the absence of substrate, hSGLT1 cannot go through a full cotransport cycle. Thus, by controlling membrane potential (V_m) and extracellular Na concentration, three distinct conformational states can be assessed: inward-facing (IF), outward-facing (OF), and outward-facing Na-bound (OF+Na). Using recent kinetic models proposed for hSGLT1 based on pre-steady-state currents (28), we can assess the probabilities of occupation for each state during experimental trials.

In the presence of external Na and with a V_m of −50 mV, the transporters are distributed between IF state (24%), OF state (56%), and OF+Na (20%) conformations. When extracellular Na is replaced by NMDG, the Na-bound state redistributes almost equally into the IF state (34%) and the OF state (66%). This is associated with a significant increase in the total P_f of hSGLT1-expressing oocytes ($p < 0.0001$, $n = 10$). However, a significant increase was also seen in noninjected oocytes ($p < 0.01$, $n = 6$) (see Fig. 5 *B*). Subtracting the P_f measured for noninjected oocytes from the P_f measured for hSGLT1-expressing oocytes, the effect of replacing external Na remains statistically significant for the hSGLT1-specific component (a specific P_f of 1.8 ± 0.3 × 10^{-4} cm s^{-1} in the presence of 67.5 mM Na and a specific P_f of 2.2 ± 0.4 × 10^{-4} cm s^{-1} in the absence of Na ($p = 0.03$, $n = 10$ paired measurements, see Fig. 5 *D*). The direction of this change also suggests that the Na-free states (OF and IF) are more permeable than the Na-bound state (OF+Na). At −100 mV in the presence of Na, 74% of the cotransporters are found in the OF+Na state. If V_m is brought to −20 mV, 49% of the cotransporters adopt the IF state whereas only 5% remains in the OF+Na state.

As shown in Fig. 5 *C*, changing membrane potential from −20 to −100 mV produces a significant reduction in the P_f of hSGLT1-expressing oocytes that is not seen with noninjected oocytes. To obtain hSGLT1-specific membrane permeability, it is necessary to subtract the water permeability of control (noninjected) oocytes under the same conditions. Fig. 5 *D* shows that the P_f specifically associated with hSGLT1 goes from 2.1 ± 0.2 × 10^{-4} cm s^{-1} at −100 mV to 3.2 ± 0.3 × 10^{-4} cm s^{-1} at −20 mV. The difference is statistically significant ($p < 0.001$, $n = 13$ paired measurements) and suggests that the Na-free configurations (OF and IF) are more water-permeable than the Na-bound configuration (OF+Na). Nevertheless, the fact that a very significant water permeability is still present when 74% of the transporter is estimated to be in the outward and Na-bound state (when V_m is −100 mV in the presence of Na) suggests that the Na-bound and Na-free conformational states are all water-permeable.

Finally, comparison of the swelling rates measured in the presence and absence of Pz, i.e., *pz* and *post* periods in Fig. 5 *A*, shows that hSGLT1-mediated water permeability accounts for 34 ± 2% (mean ± SE, $n = 23$) of total water permeability, in agreement with previously published results (2,5,6). As expected, noninjected oocytes showed no Pz-sensitive water permeability.

DISCUSSION

We have used the crystal structure of vSGLT to build a homology model for hSGLT1 and we have identified, in both structures, a pathway through which water molecules could diffuse and account for the passive water permeability that is recognized for human and rabbit SGLT1 as well as for several other Na/coupled cotransporters (10,11).

Using GCMC, we have found that up to 208 water molecules could be stably inserted into each structure. Half of these water molecules were found to form a single pathway that extends for 40 Å and connects the intracellular and extracellular milieu. Interestingly, for both vSGLT and hSGLT1, this pathway is interrupted between the sugar binding site and the extracellular solution. For vSGLT and hSGLT1, the interruptions extend for 14 Å and 4 Å, respectively. PMF calculations confirm the presence of a energy barrier that corresponds exactly to the positions where GCMC could not insert energetically stable water molecules.

Experimentally, because of its poor expression level in oocytes (14), it is not known whether vSGLT has a measurable water permeability. (In contrast, the water permeability of human and rabbit SGLT1 is easy to measure because a large fraction of the total water permeability is inhibited by Pz in oocytes expressing these proteins (5,6).) What is also not known is whether the state that corresponds to the crystal structure of vSGLT (inward-facing galactose-bound) is water-permeable. The passive water permeability was shown to be constant in the presence or absence of substrate (5,31), but there is no consensus on what is the most populated conformational state of the cotransporter in the presence of a large sugar concentration.

Recent MD articles have shown that the vSGLT crystal structure is somewhat unstable, as both Na and galactose are found to leave their respective binding sites within 9 ns of simulation for Na (32–35) and 110 ns for galactose (32,34). In a recent article from Choe et al. (32), the release of galactose is accompanied by a ~3.5-fold increase of

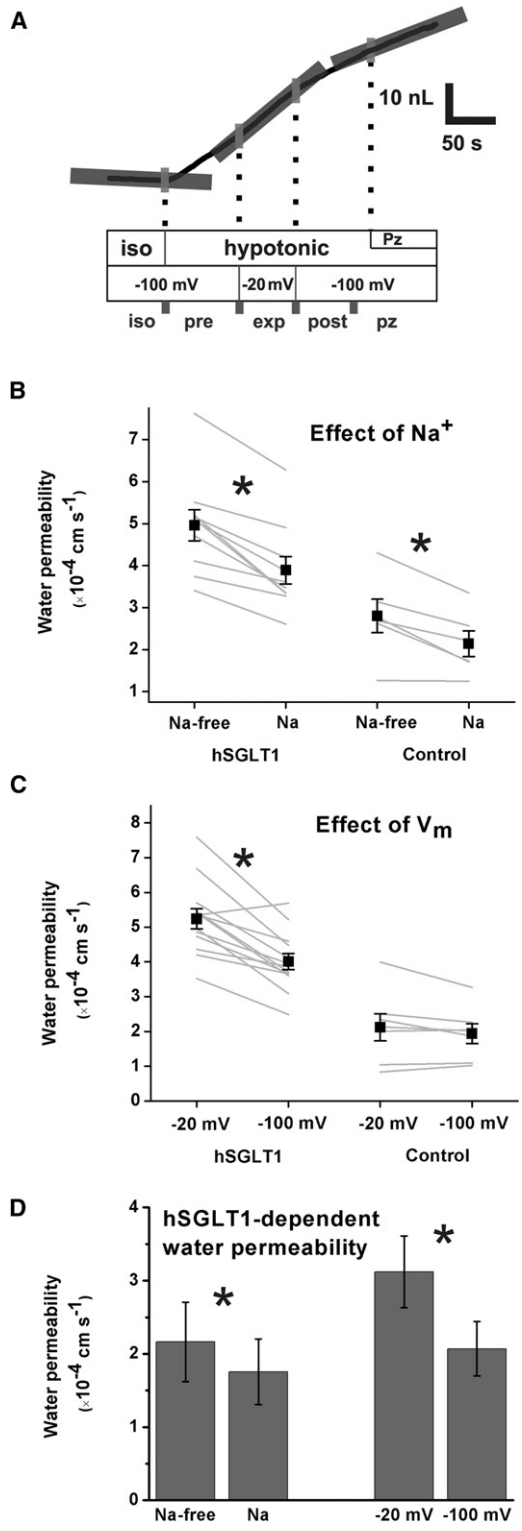

FIGURE 5 Volumetric and electrophysiological assays. (*A*) Typical assay for the effect of membrane potential. The oocyte was first stabilized in hypotonic solution (experimental condition *iso*). Hypotonic media were then superfused, while the V_m was held at −100 mV, then at −20 mV, and then at −100 mV (experimental conditions *pre*, *exp*, and *post*, respectively). Finally, the oocyte was exposed to Pz to assess the level of hSGLT1 expression (experimental condition *Pz*). Fitting of the different swelling rates (*superimposed light-shaded lines*) allowed calculation of the water permeability. A similar protocol was used to study the effect of the presence or absence of external Na. (*B*) Effect of presence of sodium on measured water permeability. Mean of measured water permeabilities for hSGLT1-injected oocytes ($n = 10$) and noninjected oocytes ($n = 6$) (*solid squares*, mean ± SE) superimposed on paired measurements for individual oocytes (*light-shaded lines*). (*C*) Effect of membrane potential on measured water permeability. Mean of measured water permeability for hSGLT1-injected oocytes ($n = 13$) and noninjected oocytes ($n = 7$) (*solid squares*, mean ± SE) superimposed on paired measurements for individual oocytes (*light-shaded lines*). (*D*) hSGLT1-dependent water permeability (mean ± SE). The effects of both V_m and of Na are statistically significant ($p < 0.001$, $n = 13$ paired measurements and $p = 0.03$, $n = 10$ paired measurements, respectively). *Statistical significance. See text for full details.

unidirectional water fluxes in both directions, suggesting that the inward-facing substrate-free configuration is significantly more water-permeable than the original crystal structure of vSGLT. It is thus possible that a modest change in the structure of the water pathway between the sugar binding site and the extracellular solution could decrease the calculated energy barrier quite significantly. For example, reorientation of residues Tyr-87 (TM2), Ala-259 (TM6E), Gln-425, Gln-428 (TM10), Phe-479 or Met-483 (TM12) for vSGLT and Phe-101, Ala-105 (TM2), Met-283, Leu-286, Thr-287 (TM6E), or Gln-455 (TM10) for hSGLT1 could produce significant changes to the pathway.

In an effort to see whether the passive water permeation pathway identified for the inward-facing configuration could apply to different conformational states, we assessed hSGLT1-dependent water permeability under different experimental conditions. We found that replacing Na by NMDG led to a small increase in water permeability, suggesting that the Na-free conformations (IF and OF) were more water-permeable than the Na-bound (OF+Na) configuration. This was pursued by changing membrane potential in the presence of Na. Based on Gagnon et al. (28), at a membrane potential of −100 mV, the pre-steady-state charge translocation indicates that 74% of the cotransporters are in the OF+Na configuration. The fact that hSGLT1-dependent P_f is only decreased by 34% (with respect to a V_m of −20 mV) confirms that the OF+Na configuration exhibits a significant P_f, though it is smaller than that of the Na-free configurations.

A different conclusion regarding the effect of Na has previously been reported by Loike et al. (2), who found that removal of extracellular Na abolished the water permeability mediated by rabbit SGLT1. In contrast to our experiments, their oocytes were preincubated in sodium-free solution for a much longer time period (30 min) than in the this study (1 min). In addition, because the swelling rate was measured for 45 min, the difference in the average swelling rates between Na-containing and Na-free solutions becomes visible only after 10 min. We interpret these results as indicating that Na has only a minor influence on hSGLT1 water permeability (no measurable initial effects) but that

prolonged exposure of oocytes to Na-free conditions produces secondary effects that affect water permeability in some other manner. In summary, although Na-free configurations are slightly more water-permeable than the outward-facing Na-bound configuration, both states are permeable and the identified water pathway seems to maintain some of its function in the different conformations of the transporter.

Over the past several years, different mechanisms have been proposed concerning the means by which SGLT1-mediated glucose cotransport can stimulate water flux. Three different views have been proposed to explain the apparent coupling between glucose and water transport: the water cotransport hypothesis (9,10,36); the middle compartment hypothesis (37,38); and the local osmotic gradient hypothesis (5,11,12). Although glucose was not involved in the numerical simulations presented above, the localization of stable water molecules in the cotransporter can shed new light on this issue.

The first view suggests that water is physically cotransported (i.e., active pumping) with Na and glucose, with reported stoichiometries of >200 and >380 water molecules per glucose molecule for hSGLT1 and rabbit SGLT1, respectively (9,10,36). According to this hypothesis, when hSGLT1 is expressed in an oocyte, the initial water flux observed (in the first 2 min) is due to water cotransport and, as an osmotic gradient progressively builds, the steady-state water movement becomes mediated (in equal parts) by water cotransport, passive water transport through the hSGLT1 water permeability, and passive water transport through the oocyte endogenous water permeability. Explaining the putative water cotransport with the alternating access mechanism would require the presence of an intramolecular cavity capable of accommodating two Na, one glucose, and at least 380 water molecules. This cavity would first need to be open to the extracellular side to fill up with water molecules. After conformational change, the filled cavity would pinch off from the extracellular side and open to the intracellular side. Then the cavity would need to reduce its volume to expel 380 water molecules to the intracellular side. Finally, it would need to somehow return to its initial state with minimal backward water movement. Our observation that hSGLT1 can accommodate only 98 water molecules in the entire pathway (as shown in Fig. 2 *B*) makes it very unlikely that a cavity at least four-times larger could exist in any of the configurations adopted by this cotransporter.

In a recent article, Choe et al. (32) reported that, during a 200-ns molecular dynamics simulation based on the vSGLT crystal structure, galactose would spontaneously exit its binding site and forces a net flux of 70–80 water molecules toward the intracellular milieu. The authors suggest that the galactose molecule would play the role of a *Brownian piston*. Although this tends to support the water cotransport hypothesis, the interpretation given by the authors should be taken with caution:

First, it would be difficult to scale-up this efflux of 70–80 water molecules per glucose in vSGLT to account for the net movement of >380 water molecules per glucose in the case of rabbit SGLT1.

Second, examination of the net count of transported water molecules during the 200-ns simulation (see Fig. 2 of Choe et al. (32) shows that the net flux is only transient. The 70–80 water molecules entering the intracellular space within 60 ns after galactose release are compensated for by a net flux in the opposite direction during the next 50 ns. Thus, we disagree that this observation can be used to support or disprove the secondary active water transport hypothesis.

The two other theoretical frameworks propose passive water permeation mechanisms that are driven by transport-dependent osmotic gradients:

One passive mechanism is based on a three-compartment model that was originally proposed to explain isosmotic *trans*-epithelial water transport. In this model, solutes are transported into a middle compartment (possibly the intercellular space in the original context) where some local hypertonicity develops and drives water flux from the apical milieu to the middle compartment. The water displacement produces an increase in the middle compartment pressure, which drives the solution toward the basolateral side of the epithelium. This model has been proposed to apply to the cotransporter-mediated water flux (37,38), which raises significant difficulties. The original three compartment model needs to be downscaled by four orders of magnitude, and it is unclear how any significant osmotic gradient could be maintained within distances of ~20 Å. Also, no *middle-compartment* could be observed inside the available crystal structure of vSGLT or in the homology model for hSGLT1.

A second passive mechanism suggests that an osmotic gradient is created by cotransport flux into the intracellular unstirred layer (5,11,12). This hypothesis is the simplest default hypothesis, assuming only that the cotransporter molecule exhibits a passive permeation pathway for water. This hypothesis is supported by the fact that a transmembrane osmotic gradient of the adequate amplitude was experimentally detected as soon as 20 s after initiating the cotransport mechanism. Once the osmotic gradient is set up, water flow occurs through all available water permeation pathways including the passive pathway through the cotransporter itself. The water distribution within the cotransporter molecule that was revealed in this study is consistent with this view of glucose-driven water transport. The pathways observed through the vSGLT crystal structure and the hSGLT1 homology model displayed constriction zones characterized to different extents by both GCMC and PMF calculations. PMF calculations along the identified water permeation pathway displayed a reasonable energy barrier that would allow the passive transport of water and is fully consistent with the experimental data obtained on rabbit SGLT1 (3,6).

CONCLUSION

The recent crystallization of vSGLT allowed investigation of the structural basis for water permeation through both vSGLT and the homologous hSGLT1 using GCMC/MD simulations and PMF calculations. Insertion of stable water molecules in both vSGLT and hSGLT1 identified water permeation pathways from the intracellular to extracellular milieu. These pathways comprise ~100 water molecules in the protein interior and display constriction zones between the sugar binding site and the extracellular space. This provides a structural basis for the passive water permeability associated with SGLT1, and makes the water cotransport hypothesis very difficult to rationalize. PMF calculations for water permeation through the crystal structure of vSGLT reveal the presence of a ~8 kcal mol^{-1} energy barrier, in good agreement with previous measurements on rabbit SGLT1. Volumetric and electrophysiological measurements performed on hSGLT1 show that the conformational state in which vSGLT was crystallized is water-permeable, and suggests that the identified water permeation pathway is also present in other conformations.

SUPPORTING MATERIAL

One figure is available at http://www.biophysj.org/biophysj/supplemental/S0006-3495(11)01077-0.

The authors are grateful to Drs. Chunfeng Zhao and Yulia Subbotina for their help with GCMC and MD simulations and Dr. Benoit Roux for helpful comments on the manuscript.

This work was funded by Discovery Grants from the National Sciences and Engineering Council (RGPIN-315019 and RGPIN-380738) to S.N. and J.Y.L., respectively. S.N. is a recipient of the Alberta Innovates Technology Futures New Faculty and the Canadian Institute for Health Research New Investigator grants.

REFERENCES

1. Fischbarg, J., K. Y. Kuang, …, J. Loike. 1989. Evidence that the glucose transporter serves as a water channel in J774 macrophages. *Proc. Natl. Acad. Sci. USA*. 86:8397–8401.
2. Loike, J. D., S. Hickman, …, J. Fischbarg. 1996. Sodium-glucose cotransporters display sodium- and phlorizin-dependent water permeability. *Am. J. Physiol.* 271:C1774–C1779.
3. Loo, D. D., T. Zeuthen, …, E. M. Wright. 1996. Cotransport of water by the Na^+/glucose cotransporter. *Proc. Natl. Acad. Sci. USA*. 93: 13367–13370.
4. Wright, E. M., B. A. Hirayama, and D. F. Loo. 2007. Active sugar transport in health and disease. *J. Intern. Med.* 261:32–43.
5. Duquette, P. P., P. Bissonnette, and J. Y. Lapointe. 2001. Local osmotic gradients drive the water flux associated with Na^+/glucose cotransport. *Proc. Natl. Acad. Sci. USA*. 98:3796–3801.
6. Loo, D. D., B. A. Hirayama, …, E. M. Wright. 1999. Passive water and ion transport by cotransporters. *J. Physiol.* 518:195–202.
7. Reuss, L., and B. H. Hirst. 2002. Water transport controversies—an overview. *J. Physiol.* 542:1–2.
8. Schultz, S. G. 2001. Epithelial water absorption: osmosis or cotransport? *Proc. Natl. Acad. Sci. USA*. 98:3628–3630.
9. Loo, D. D., E. M. Wright, and T. Zeuthen. 2002. Water pumps. *J. Physiol.* 542:53–60.
10. Zeuthen, T., A. K. Meinild, …, D. A. Klaerke. 2001. Isotonic transport by the Na^+-glucose cotransporter SGLT1 from humans and rabbit. *J. Physiol.* 531:631–644.
11. Charron, F. M., M. G. Blanchard, and J. Y. Lapointe. 2006. Intracellular hypertonicity is responsible for water flux associated with Na^+/glucose cotransport. *Biophys. J.* 90:3546–3554.
12. Gagnon, M. P., P. Bissonnette, …, J. Y. Lapointe. 2004. Glucose accumulation can account for the initial water flux triggered by Na^+/glucose cotransport. *Biophys. J.* 86:125–133.
13. Faham, S., A. Watanabe, …, J. Abramson. 2008. The crystal structure of a sodium galactose transporter reveals mechanistic insights into Na^+/sugar symport. *Science (NY).* 321:810–814.
14. Leung, D. W., E. Turk, …, E. M. Wright. 2002. Functional expression of the *Vibrio parahaemolyticus* Na^+/galactose (vSGLT) cotransporter in *Xenopus laevis* oocytes. *J. Membr. Biol.* 187:65–70.
15. Lomize, M. A., A. L. Lomize, …, H. I. Mosberg. 2006. OPM: orientations of proteins in membranes database. *Bioinformatics.* 22:623–625.
16. Canutescu, A. A., A. A. Shelenkov, and R. L. Dunbrack, Jr. 2003. A graph-theory algorithm for rapid protein side-chain prediction. *Protein Sci.* 12:2001–2014.
17. Baker, D., and A. Sali. 2001. Protein structure prediction and structural genomics. *Science.* 294:93–96.
18. Ginalski, K. 2006. Comparative modeling for protein structure prediction. *Curr. Opin. Struct. Biol.* 16:172–177.
19. Noskov, S. Y. 2008. Molecular mechanism of substrate specificity in the bacterial neutral amino acid transporter LeuT. *Proteins.* 73:851–863.
20. Jo, S., J. B. Lim, …, W. Im. 2009. CHARMM-GUI Membrane Builder for mixed bilayers and its application to yeast membranes. *Biophys. J.* 97:50–58.
21. Im, W., S. Jo, …, V. G. Iyer. 2008. Software news and updates—CHARMM-GUI: a web-based graphical user interface for CHARMM. *J. Comput. Chem.* 29:1859–1865.
22. Brooks, B. R., C. L. Brooks, 3rd, …, M. Karplus. 2009. CHARMM: the biomolecular simulation program. *J. Comput. Chem.* 30:1545–1614.
23. Woo, H. J., A. R. Dinner, and B. Roux. 2004. Grand canonical Monte Carlo simulations of water in protein environments. *J. Chem. Phys.* 121:6392–6400.
24. Im, W., S. Bernèche, and B. Roux. 2001. Generalized solvent boundary potential for computer simulations. *J. Chem. Phys.* 114:2924–2937.
25. Wang, J. Y., Y. Q. Deng, and B. Roux. 2006. Absolute binding free energy calculations using molecular dynamics simulations with restraining potentials. *Biophys. J.* 91:2798–2814.
26. Bissonnette, P., J. Noël, …, J. Y. Lapointe. 1999. Functional expression of tagged human Na^+-glucose cotransporter in *Xenopus laevis* oocytes. *J. Physiol.* 520:359–371.
27. Longpré, J.-P., D. G. Gagnon, …, J.-Y. Lapointe. 2010. The actual ionic nature of the leak current through the Na^+/glucose cotransporter SGLT1. *Biophys. J.* 98:231–239.
28. Gagnon, D. G., C. Frindel, and J. Y. Lapointe. 2007. Effect of substrate on the pre-steady-state kinetics of the Na^+/glucose cotransporter. *Biophys. J.* 92:461–472.
29. Bourgeois, F., M. J. Coady, and J. Y. Lapointe. 2005. Determination of transport stoichiometry for two cation-coupled myo-inositol cotransporters: SMIT2 and HMIT. *J. Physiol.* 563:333–343.
30. Zampighi, G. A., M. Kreman, …, E. M. Wright. 1995. A method for determining the unitary functional capacity of cloned channels and transporters expressed in *Xenopus laevis* oocytes. *J. Membr. Biol.* 148:65–78.
31. Meinild, A., D. A. Klaerke, …, T. Zeuthen. 1998. The human Na^+-glucose cotransporter is a molecular water pump. *J. Physiol.* 508:15–21.
32. Choe, S., J. M. Rosenberg, …, M. Grabe. 2010. Water permeation through the sodium-dependent galactose cotransporter vSGLT. *Biophys. J.* 99:L56–L58.

33. Li, J., and E. Tajkhorshid. 2009. Ion-releasing state of a secondary membrane transporter. *Biophys. J.* 97:L29–L31.

34. Watanabe, A., S. Choe, …, J. Abramson. 2010. The mechanism of sodium and substrate release from the binding pocket of vSGLT. *Nature*. 468:988–991.

35. Zomot, E., and I. Bahar. 2010. The sodium/galactose symporter crystal structure is a dynamic, not so occluded state. *Mol. Biosyst.* 6:1040–1046.

36. Zeuthen, T., B. Belhage, and E. Zeuthen. 2006. Water transport by Na^+-coupled cotransporters of glucose (SGLT1) and of iodide (NIS). The dependence of substrate size studied at high resolution. *J. Physiol.* 570:485–499.

37. Naftalin, R. J. 2010. Reassessment of models of facilitated transport and cotransport. *J. Membr. Biol.* 234:75–112.

38. Naftalin, R. J. 2008. Osmotic water transport with glucose in GLUT2 and SGLT. *Biophys. J.* 94:3912–3923.